TF Linear Motor with Passive Guideway for Low Speed Transport

No. 075

Mauro Andriollo, Manuel De Bortoli, Giovanni Martinelli, Augusto Morini and Andrea Tortella
Department of Electrical Engineering, University of Padova, Italy
mauro.andriollo, manuel.debortoli, augusto.morini, giovanni.martinelli@unipd.it

ABSTRACT: Linear motors are frequently proposed for the propulsion of low speed transport systems such as short-haul passenger transport in public areas or in urban light transit systems. In this paper an innovative configuration of a modular transverse flux permanent magnet (PM) motor with variable reluctance secondary is presented, with both windings and PMs placed on the mover. The thrust performance are evaluated by analyzing a simplified 2D model and compared with the ones related to a surface mounted PM motor, the same active width and length of the mover being maintained. In particular, the influence of the tooth profile on the thrust average value and ripple is taken into consideration to optimize the motor configuration.

1 INTRODUCTION

The linear motor applications in low speed transport systems are by now well–established from the technological point of view and very competitive with the conventional rotary motors-based systems as regards the performances and the reliability. Typical utilizations are in factory logistics or for short-haul passenger transport in public areas (expositions, airport terminals), characterized by a maximum run of some kilometers, payload from some tens to several hundreds of kilograms and a maximum speed of about 10 m/s, (Gieras & Piech 2000, Kang & Weh 2004).

As regards the electromagnetic structure, a configuration with windings placed along the guideway allows to increase the payload (only excitation PMs on board), to improve the apparatus reliability (absence of sliding contacts) and the dynamical performances. On the other side, the transverse flux linear hybrid reluctance motor (TF-LHRM) with a purely passive ferromagnetic secondary, proposed in this paper, represents a particularly profitable option, since the absence of stator windings allows a remarkable saving in building the guideway and an appreciable efficiency improvement. The proposed configuration (Figs.1a-b) has a moving primary consisting of an iron core 3-phase winding and a double array of permanent magnets (PMs) placed inside open slots.

The opposite sides of the secondary are displaced by a half-pitch. The modulation of the excitation PMs alternating flux by the 3-phase winding mmf produces the thrust by the electromagnetic Vernier effect (Mueller 2003). The guideway assembly can be eased by manufacturing the stator poles in “halved C”-shaped lamination stacks grafted together on a solid iron base.

The influence of the stator and mover tooth profile on the thrust performance is evaluated by a FEM analysis (FEA) of a 2D simplified model, taking anyway into account the end winding effects by 2D analyses of suitable transversal cross sections.

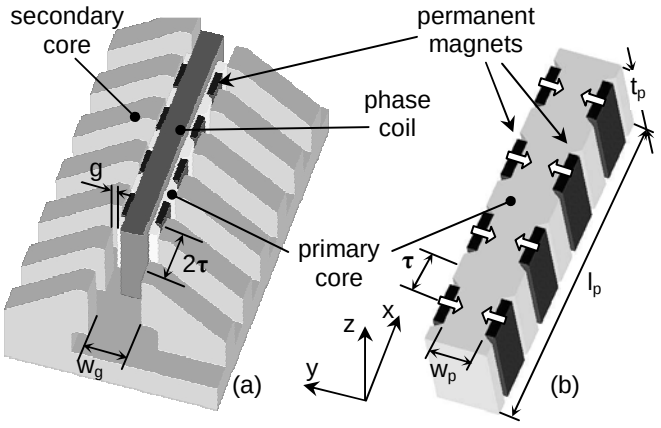

Figure 1. a) Partial view of a TF-LHRM (single phase module); b) detail of the moving primary, without the phase coil for the sake of clearness.

The TF-LHRM performances will be compared with the ones related to a surface mounted PM motor with a conventional PM array with opposite magnetization, requiring a double PM amount.

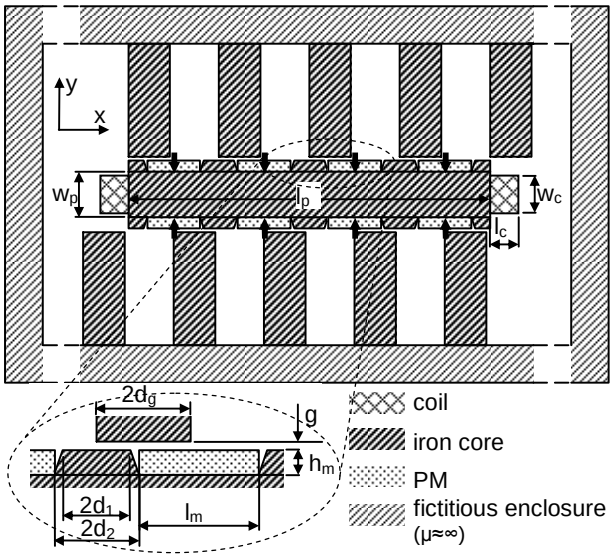

Figure 2. Simplified TF-LHRM model for the 2D FEA, with some geometric quantities highlighted.

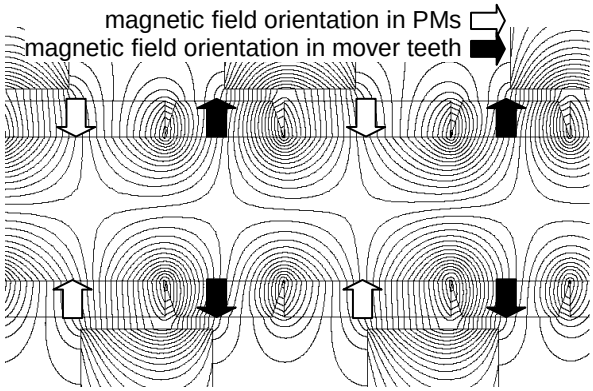

Figure 3. Flux lines related to a no-load condition.

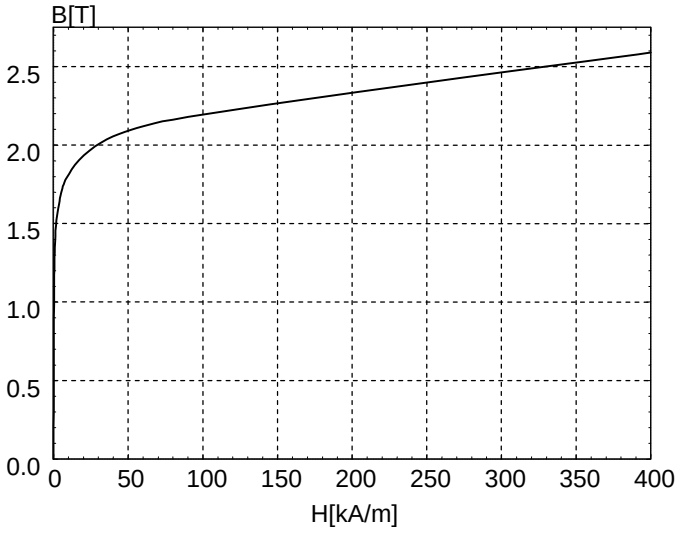

Figure 4. B-H characteristic of the iron core.

2 MOTOR CONFIGURATION

Figure 2 shows the simplified model adopted for the 2D electromagnetic analysis, allowing a preliminary investigation of the influence of the most significant geometric parameters, a reasonable calculation time being maintained. To reproduce the effect of the ferromagnetic base of the actual 3D structure, the 2D configuration is enclosed in a fictitious yoke with very high permeability, suitably sized not to alter the field distribution in the air gap region. The PMs placed on the same mover side have concordant magnetization, while the two faced PM arrays are oppositely magnetized. Consequently, the mover teeth act as complementary poles with respect to the PMs, as exemplified in Figure 3 (black arrows). The model represents a single phase module. The operation of the whole motor can be reproduced by summing the effects of the three phase modules, assuming their axes are evenly spaced along the motion direction x by the distance $d_{ph}=2\tau(k\pm1/3)$, with k integer (i.e. by 120 electrical degrees), and supplied by a three phase symmetric set of sinusoidal currents. Such approach applies provided that electromagnetic interaction among the modules is negligible, as it can be verified by the analysis of the whole three-phase configuration (requiring a remarkably higher number of mesh elements and consequently a greater calculation time).

The distribution of the flux lines shown in Figure 3 highlights the influence of the stator and mover tooth profiles, affecting both the reluctance contribution to the thrust and the permeance of the PM flux paths; in particular, the inclination of mover tooth sides and their distance from the PMs heavily influence the leakage fluxes of the PMs themselves.

According to such considerations, the geometric parameters d_1, d_2, d_g, related to the mover and stator tooth profiles and l_m (magnet width) can be regarded as the most significant with respect to the electromagnetic performance, provided that the air gap g is maintained to the minimum feasible value and the PM height h_m is fixed taking into account demagnetization due the reaction armature mmf. The starting configuration (denoted by "0" in the following) is defined according to the *B-H* characteristic of Figure 4 and to the data reported in Table I.

Table 1. Main data of the TF-LHRM starting configuration.

sizes [mm] (Figs.1, 2)	τ=24, g=2, w_p=24, l_p=192, w_g=40, d_1=d_2=d_g=12, l_c=15, w_c=20, h_m=6, l_m=24, t_p=60, d_{ph}=224
MP coercivity H_c [kA/m]	−890
MP retentivity B_r [T]	1.23
rated phase mmf nI [A_{rms}]	1600
current density J [A/mm^2]	7.6
enclosure rel. permeability	10^4

3 PARAMETRIC ANALYSIS

The influence of the above mentioned geometric parameters is investigated taking into account three aspects related to the motor performance:

- the thrust average value $\langle F_x \rangle$;
- the thrust ripple r_{Fx} (maximum deviation of the instantaneous value with respect to $\langle F_x \rangle$);
- the average thrust/mover mass $\langle F_x \rangle / M_m$ ratio.

Furthermore, to avoid the PM demagnetization risk, the minimum value $B_{y,min}$ of the flux density component along y in the PMs is checked for each configuration. The thrust instantaneous value is evaluated by an automated FEA sequence (Ansoft 2005) applied to the model of Figure 2, for a convenient set of values of the relative mover-stator position x_0 (Figures 2 and 3 correspond to x_0=0, with a null no-load coil flux linkage). The phase mmf ni is varied as a function of x_0 according to the relation:

$$ni = \sqrt{2}\, nI \cos\left(\frac{\pi x_0}{\tau} - \gamma\right) \tag{1}$$

The reference load condition considered in the following corresponds to the rated current value and to γ=0° (armature mmf in quadrature with respect to the no-load flux linkage).

The single module thrust is calculated for 24 regularly spaced x_0 values (corresponding to an angular step of 15 electrical degrees) in the range [0,τ]. These values are then interpolated by a trigonometric polynomial $f_x(x_0)$ expressed as (Andriollo et al., 2003a):

$$f_x(x_0) = \langle f_x \rangle + \sum_{k=1}^{h} f_{x,k} \cos\left(k \frac{2\pi x_0}{\tau} + \phi_k\right) \tag{2}$$

considering the first h=7 harmonics. The resulting force for a complete three-phase set is then given by:

$$F_x(x_0) = 3\langle f_x \rangle + 3\sum_{k'=1}^{\lfloor h/3 \rfloor} f_{x,k'} \cos\left(3k' \frac{2\pi x_0}{\tau} + \phi_{3k'}\right) \tag{3}$$

since all but the harmonics with order multiple of 3 are cancelled. According to (3), $\langle F_x \rangle = 3\langle f_x \rangle$ and the ripple can be determined.

3.1 Comparison of the TF-LHRM performances with the ones related to a mover with surface mounted PMs

For a preliminary estimation of the TF-LHRM design effectiveness, the performances related to the "0" mover configuration are compared with ones related to a surface mounted PM (SPM) mover. This configuration is obtained by replacing the mover teeth with PMs having the same sizes of the preexistent ones and opposite magnetization (resulting in a double PM amount, 1.02 kg instead of 0.51 kg). Figure 5 evidences that the performances of the TF-LHRM are better than the ones of SPM configuration (denoted by the S1 subscript) as for both the thrust average value and its ripple. The thrust performance is quantitatively defined by the values of the significant quantities {$\langle F_{x0} \rangle$=801 N, M_{m0}=14.2 kg, $\langle F_{x0} \rangle / M_{m0}$=56.5 N/kg, r_{Fx0}=7.2%} for the TF-LHRM configuration and {$\langle F_{xS1} \rangle$= 747 N, M_{mS1}=14.1 kg, $\langle F_{xS1} \rangle / M_{mS1}$=53.0 N/kg, r_{FxSM1}=17.0%} for the SPM mover.

3.2 Variation of the mover tooth profile (d_1, d_2 parameters) with fixed PM width (l_m=const.)

In the preliminary parametric analysis, only the mover tooth geometry is involved, the PM and guideway configuration being unvaried. A trapezoidal tooth profile is considered, with the constraint $d_1 \le d_2 \le \tau/2$. Figures 6-8 show the results of this analysis.

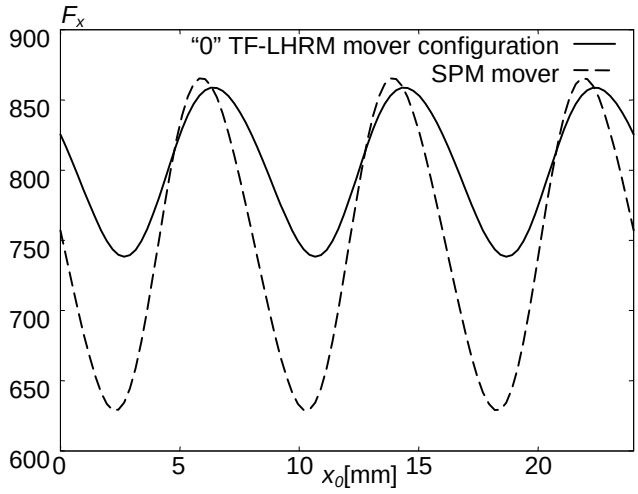

Figure 5. Comparison of the instantaneous thrust values for the starting TF-LHRM mover configuration and for SPM mover.

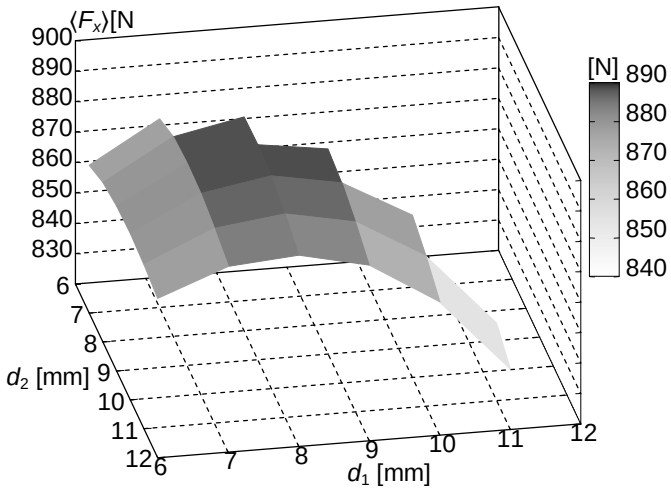

Figure 6. Thrust average value $\langle F_x \rangle$ as a function of the mover tooth geometric parameters d_1 and d_2.

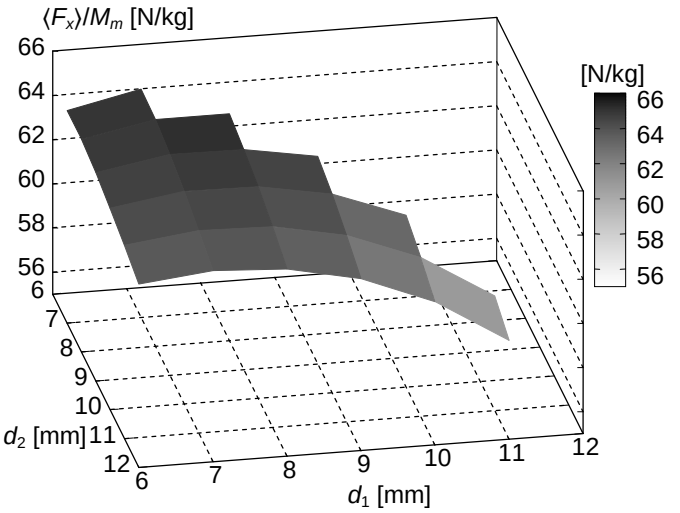

Figure 7. Thrust average value/mover mass ratio $\langle F_x \rangle / M_m$ as a function of the mover tooth geometric parameters d_1 and d_2.

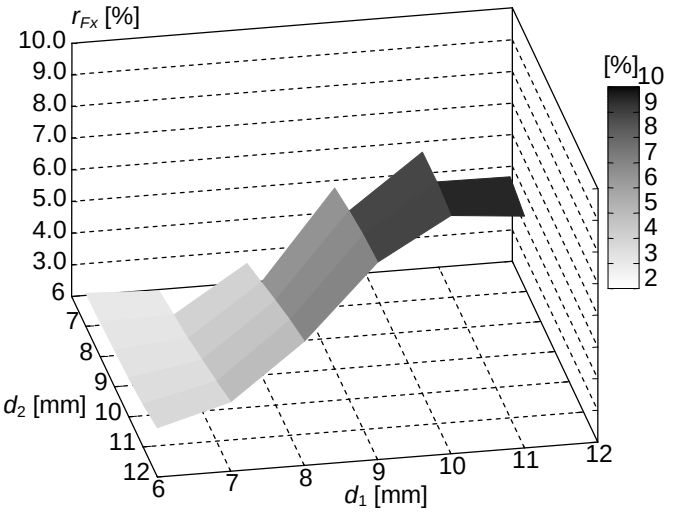

Figure 8. Thrust ripple r_{Fx} as a function of the mover tooth geometric parameters d_1 and d_2.

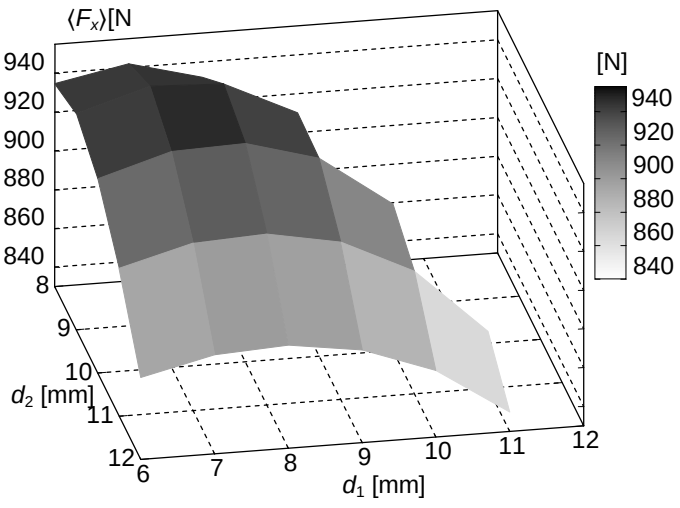

Figure 9. Thrust average value $\langle F_x \rangle$ as a function of the mover tooth geometric parameters d_1 and d_2.

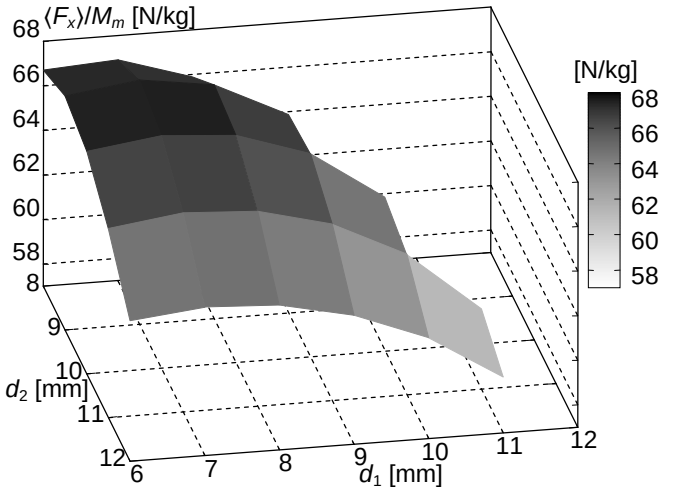

Figure 10. Thrust average value/mover mass ratio $\langle F_x \rangle / M_m$ as a function of the mover tooth geometric parameters d_1 and d_2.

From the point of view of the pure thrust performance, Figure 6 shows that the maximum of $\langle F_x \rangle$ is achieved in the range 7 mm$\leq d_1$, $d_2 \leq$9 mm. As for the specific thrust, i.e. the average thrust/mover mass ratio $\langle F_x \rangle / M_m$ (Fig. 7), the best results are obtained for 6 mm$\leq d_1$, $d_2 \leq$8 mm. Such range of values is convenient also to reduce the thrust ripple r_{Fx}, as shown by Figure 8. A good compromise among the various performance requirements is achieved for d_1=d_2=7 mm, (mover configuration denoted by the A subscript in the following as a reference for the following analyses). As regards the thrust performance, the values of the significant quantities for this configuration are $\{\langle F_{xA} \rangle$=882 N, $\langle F_{xA} \rangle / M_{mA}$=65.3 N/kg, r_{FxA}=2.9%$\}$, with an appreciable improvement with respect to the starting configuration.

3.3 Variation of the mover tooth profile (d_1, d_2 parameters) and of the PM width (l_m=2(τ−d_2))

Since the former analysis shows the convenience of the mover tooth narrowing, as a further development, the PM width is varied to fill the whole slot extension, i.e. l_m=2(τ−d_2), maintaining the constraint $d_1 \leq d_2 \leq \tau/2$ and varying the mover tooth parameters in the ranges 6 mm$\leq d_1 \leq$12 mm, 8 mm$\leq d_2 \leq$12 mm.

The Figures 9-11 show the influence of the parametric variation on the thrust performance: the best performance for the thrust average value and the thrust/mover mass ratio is obtained for 6 mm$\leq d_1 \leq$8 mm, 8 mm$\leq d_2 \leq$10 mm (Figs. 9,10), while the lowest ripple is obtained for d_1+$d_2 \approx$18 mm (Fig. 11). As a compromise, the mover configuration with d_1=8 mm, d_2=10 mm, l_m=28 mm is chosen as a new reference (denoted by the B subscript in the following). The corresponding values of the significant performances quantities are $\{\langle F_{xB} \rangle$=943 N, $\langle F_{xB} \rangle / M_{mB}$=67.2 N/kg, r_{FxB}=1.4%$\}$.

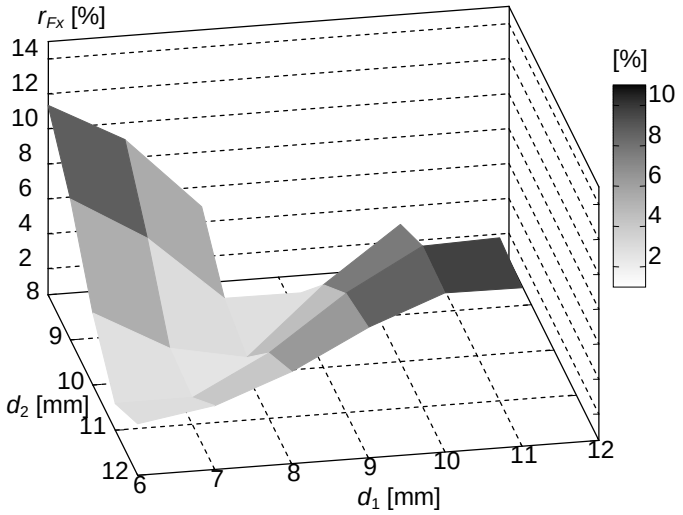

Figure 11. Thrust ripple r_{Fx} as a function of the mover tooth geometric parameters d_1 and d_2.

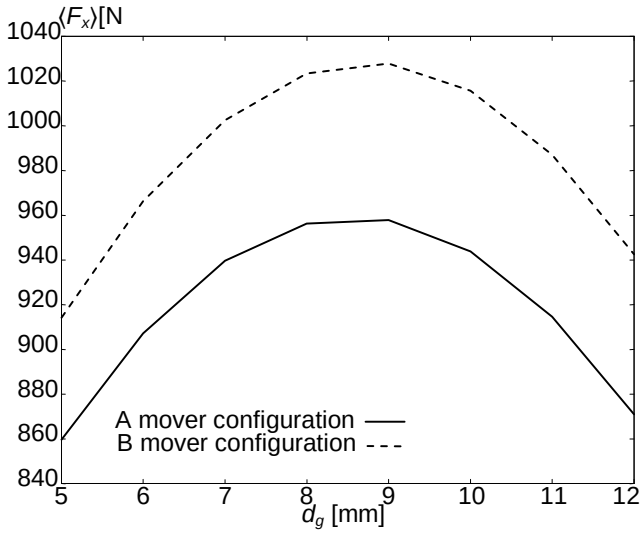

Figure 12. Thrust average value ⟨F_x⟩ as a function of the stator tooth width d_g for the A and B mover configurations.

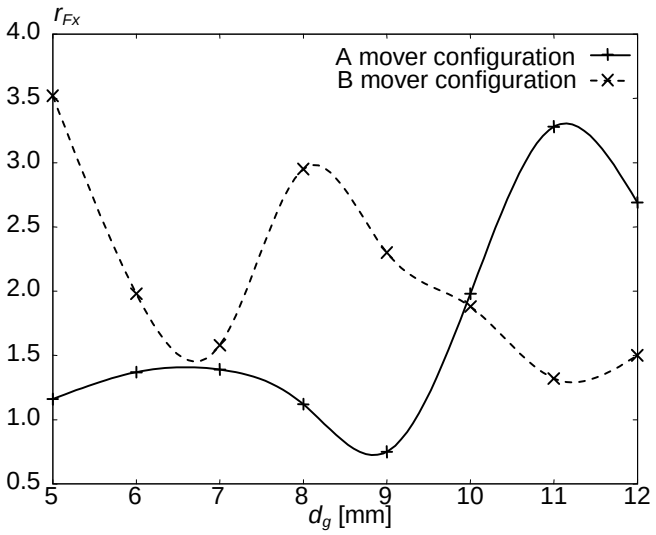

Figure 13. Thrust ripple r_{Fx} as a function of the stator tooth width d_g for the A and B mover configurations.

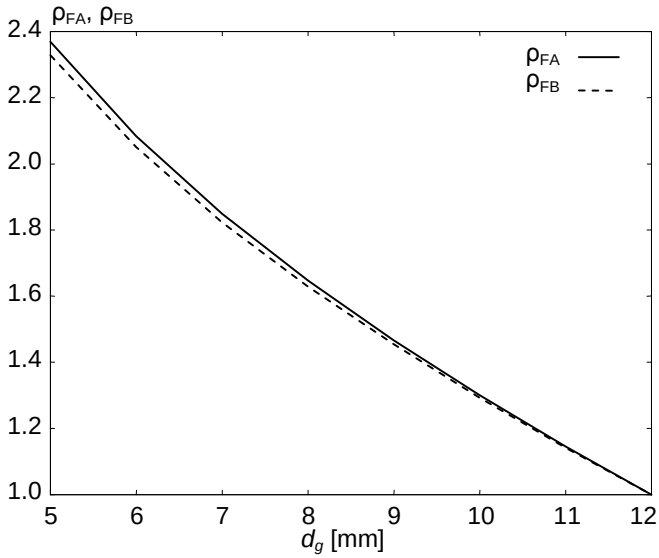

Figure 14. Guideway design effectiveness for the A and B mover configurations (ρ_{FA}, ρ_{FB}) as a function of d_g.

3.4 Variation of the stator tooth width (d_g parameter), d_1, d_2 and l_m being unvaried

Finally, the influence of the stator tooth width d_g was investigated, the mover parameters being maintained to the values corresponding to A (d_1=d_2=7 mm, l_m=24 mm) or B configuration (d_1=8 mm, d_2=10 mm, l_m=28 mm). The results of the analysis are reported in Figures 12-14. As for the thrust average value, Figure 12 shows a remarkable improvement for both the mover configurations, reducing d_g from the starting value of 12 mm to about 9 mm. From the point of view of the thrust ripple (Fig. 13), the reduction of d_g from 12 to 9 mm generally results in a remarkable improvement for the A configuration (from 7.2% to 0.75%) and in a worsening for the B configuration (from 1.4% to 2.4%). Since the guideway tooth mass can be assumed directly proportional to d_g, the ratio $\langle F_x\rangle/d_g$ can be considered as an index related to the effectiveness of the guideway design.

Figure 14 shows the relative values of this index $\rho_{FA}=(\langle F_x\rangle/d_g)/(\langle F_{xA}\rangle/d_{g0})$ and $\rho_{FB}=(\langle F_x\rangle/d_g)/(\langle F_{xB}\rangle/d_{g0})$ for the A and B mover configurations with respect to the basis values $\langle F_{xA}\rangle/d_{g0}$ and $\langle F_{xB}\rangle/d_{g0}$, corresponding to the starting value d_{g0}=12 mm of the guideway tooth width. Even though the performance of the guideway design improves as d_g decreases, the contraction of the stator tooth width shouldn't worsen excessively the thrust performance. According to such considerations, the value d_g=7 mm and the values related to the B mover geometry are adopted for the final configuration (C subscript): its performance is defined by the set of values {$\langle F_{xC}\rangle$=1003 N, $\langle F_{xC}\rangle/M_{mB}$=71.4 N/kg, r_{FxC}=1.6%, ρ_{FC}=1.82}.

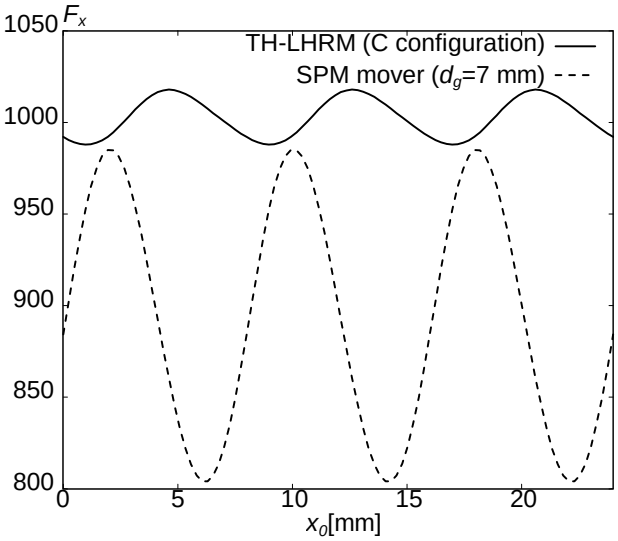

Figure 15. Thrust instantaneous values related to the C TF-LHRM configuration and to the SPM mover (d_g=7 mm).

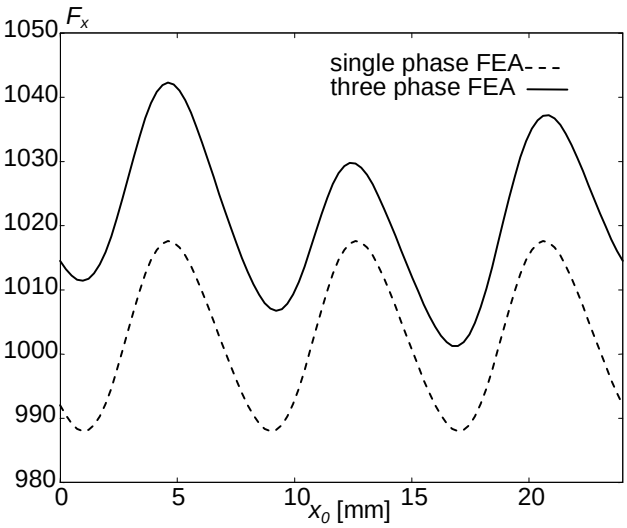

Figure 16. Thrust instantaneous values obtained by 2D FEAs of a single phase model and of the complete three-phase model.

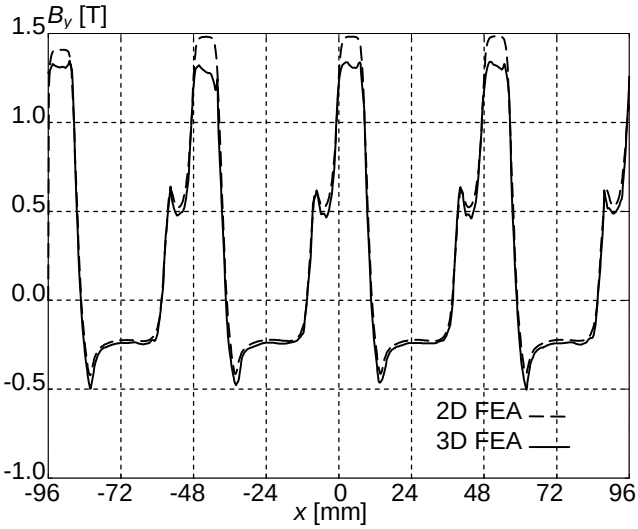

Figure 17. Flux density values obtained by 2D and 3D FEAs as functions of x along a line in the center of the air gap (x_0=0 mm).

Figure 15 allows comparing the instantaneous thrust values of the C configuration with the ones related to the initial SPM mover configuration and with the same guideway geometry (d_g=7 mm): the superiority of the TF-LHRM performances with respect to the SPM mover is confirmed. The values for the latter configuration are {$\langle F_{xS2}\rangle$= 894 N, $\langle F_{xS2}\rangle/M_{mS1}$=53.0 N/kg, r_{FxS2}=10.2%}.

4 IMPACT OF THE SIMPLIFYING HYPOTHESES

The impact of various assumptions adopted to simplify the analysis and to reduce the calculation time is now investigated, considering the final configuration located by means of the parametric analysis.

4.1 Magnetic interaction among the phase modules

The hypothesis that the three phase modules don't interact with each other is tested by comparing the instantaneous values of the thrust obtained by combining the results related to a single phase FEA and the ones related to a FEA of the complete three-phase model (Fig. 16): on the whole, the difference between the values is relatively constant and about 2%.

4.2 Influence of the three dimensionality

Figures 1 and 2 suggest that the side effects (i.e., the dependence on the z coordinate) cannot be undoubtedly neglected, provided that the t_p size is not very large in comparison with w_g. The 2D and the 3D models, related to a single phase module and to the same geometric and electromagnetic configuration, are therefore analyzed and the corresponding results are compared: as for the component B_y along y of the flux density (Fig. 17, at the reference load, with x_0=0 mm; the mover centre is the reference frame origin), the difference between 2D and 3D FEAs is rather limited and localized near the peak values.

The side effects are recognizable in Figure 18, where B_y is reported as a function of z. Also the difference between the thrust instantaneous values is relatively low (Fig. 19), with the average value about the 5% lower in the 3D model. Figures 20 and 21 allow to compare the instantaneous values of the side force component F_y and the yawing torque component T_z obtained by a sequence of 2D and 3D FEAs, for different mechanical arrangement of the phase modules. Assuming each phase module is independently supported to withstand the side effects due to F_y and T_z, the results obtained by the FEAs can be straightforwardly applied.

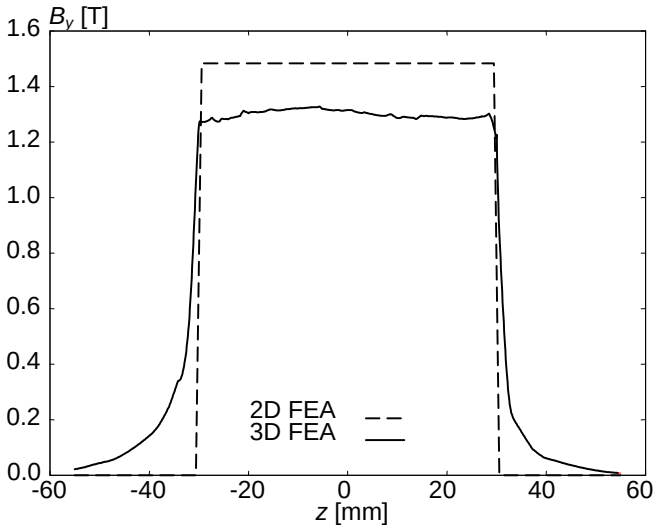

Figure 18. Flux density values obtained by 2D and 3D FEAs as functions of z in the middle of the air gap (x=4 mm).

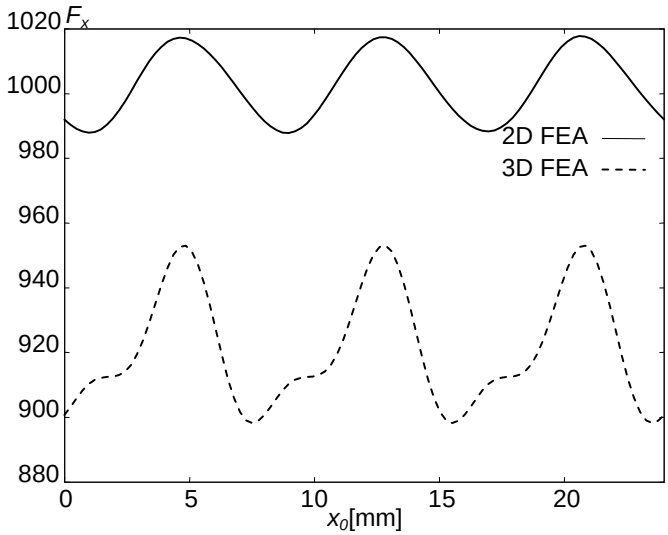

Figure 19. Comparison between the thrust instantaneous values obtained by 2D and 3D FEAs as functions of x_0.

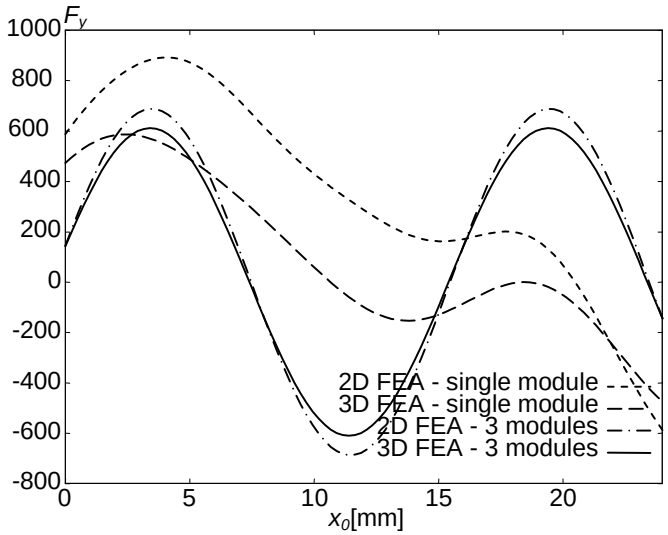

Figure 20. Side force F_y as a function of x_0, for a single module and for a 3 module assembly, obtained by 2D and 3D FEAs.

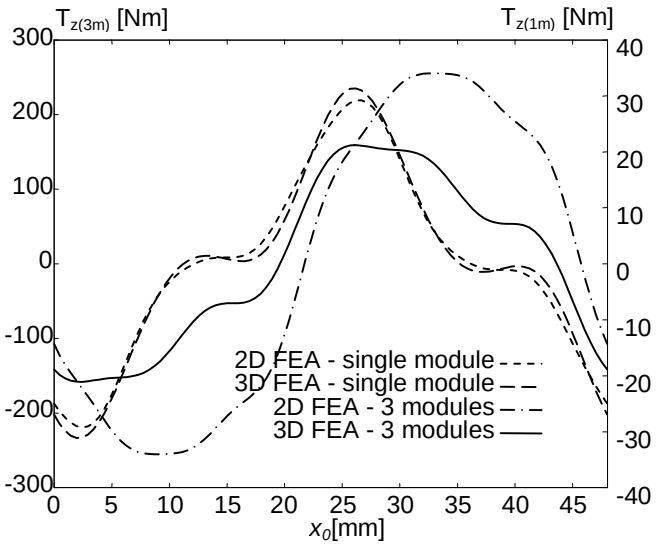

Figure 21. Yawing torque as a function of x_0, for a single module and for a 3 module assembly ($T_{z(1m)}$ and $T_{z(3m)}$, respectively), obtained by 2D and 3D FEAs.

On the contrary, if the three modules are rigidly connected together to a single support, in the resulting side force component (no mutual coupling among the phases being assumed) all but the harmonics with order multiple of 3 are cancelled, likewise in the thrust component. The remaining harmonics are triple of the corresponding ones of the single module. As for the yawing torque, let $F_y(x_0)$, $T_{z(1m)}(x_0)$ the lateral force and yawing torque acting on the phase 1 module and $T_{z(3m)}(x_0)$ the yawing torque for the 3 modules assembly as functions of the mover position x_0. It is:

$$T_{z(3m)}(x_0) = \sum_{k=1}^{3} T_{z(1m)}\left(x_0 - (k-1)d_{ph}\right) + \\ + \left(F_y\left(x_0 - 2d_{ph}\right) - F_y(x_0)\right)d_{ph} \tag{4}$$

Even if a remarkable difference is recognizable between the values of F_y of the 2D and 3D FEAs for the single module, nevertheless the concordance for the results is rather good for the 3 module set (Fig. 20; peak values are ≈12% greater in 2D than in 3D FEAs). On the contrary, the yawing torque values $T_{z(1m)}$ agree well enough (Fig. 21; peak values are ≈7% lower in 2D than in 3D FEAs), while $T_{z(3m)}$ is definitely overestimated in the 2D FEAs for the 3 modules assembly (≈+60% for the peak values with respect to the 3D FEAs), due to the F_y overvaluation.

The TF-LHRM phase inductance can be more accurately evaluated, without 3D FEAs, taking into account the end winding leakage fluxes by the FEAs of suitable 2D transversal cross sections (Fig. 22). In these models, the effect of the coil mmf in the air gap (already taken into account by the model of Figure 2) is cancelled by suitable current sheets with opposite mmf (Andriollo et al., 2003b).

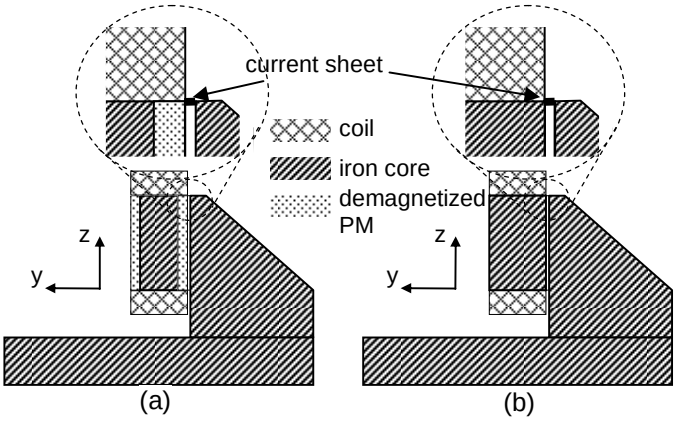

Figure 22. Transversal cross sections to take into account the end winding leakage fluxes ((a) PM cut plane, (b) mover tooth cut plane).

Table 2. Per turn coil inductances as functions of x_0.

x_0 [mm]	Λ_{3D} [μH]	Λ_{2D} [μH]	$\Lambda_{ew,2D}$ [μH]	Λ'_{2D} [μH]
0	1.397	1.080	0.323	1.403
2	1.393	1.075	0.323	1.398
4	1.371	1.061	0.323	1.384
6	1.364	1.055	0.323	1.378
8	1.366	1.057	0.323	1.380
10	1.372	1.062	0.323	1.385
12	1.377	1.065	0.323	1.388
14	1.371	1.062	0.323	1.385
16	1.360	1.056	0.323	1.379
18	1.361	1.054	0.323	1.377
20	1.370	1.062	0.323	1.385
22	1.388	1.074	0.323	1.397
24	1.400	1.080	0.323	1.403

By means of this technique the end winding contribution $\Lambda_{ew,2D}$, related to the 2D FEAs of the configurations of Figure 19, is summed to per turn coil inductance Λ_{2D} obtained by the 2D FEAs applied to the model of Fig.2, giving the total inductance Λ'_{2D}. Table 2 allows verifying the very good concordance between these refined 2D values and the corresponding values Λ_{3D} related to the 3D FEAs for different mover positions (the maximum difference is ≈1.3%).

To sum up, the results of the 2D FEAs are reliable to evaluate the thrust performance, allow at least an approximate assessment of the stresses along *y* axes and are fairly accurate as for the phase inductance, provided the end effects are taken into account by auxiliary 2D FEAs of suitable transversal cross sections.

5 CONCLUSIONS

The novel TF-LHRM configuration proposed in the paper, based on the Vernier effect, is competitive with a more conventional mover configuration with surface mounted PMs.

A suitably devised sequence of parametric 2D FEAs allowed refining the mover and guideway design with a remarkable performance improvement and a limited expense of calculation time. The comparison with the results of 3D FEAs showed the effectiveness of this technique for the design purpose. Finally, a methodology is described to refine the 2D FEA results, for the evaluation of the phase inductance with more than satisfactory accuracy.

6 REFERENCES

Gieras, J.F. & Piech, Z.J. 2000. Linear Synchronous Motors: Transportation and Automation Systems. Boca Raton (FL): CRC Press.

Kang, D.H. & Weh, H. 2004. Design of an Integrated Propulsion, Guidance, and Levitation System by Magnetically Excited Transverse Flux Linear Motor (TFM-LM). *IEEE Trans. on Energy Conversion, vol. 19, no. 3, September 2004*: 477-484.

Mueller, M.A. & Baker, N.J. 2003. Modelling the performance of the vernier hybrid machine. *IEE Proc.-Electr. Power Appl., Vol. 150, No. 6, November 2003*: 647-654.

Andriollo, M., Martinelli, G., Morini, A., Tortella, A. & Zerbetto, M. 2003a. Performance evaluation of a TF linear PM motor. *LDIA 2003, Birmingham (UK), 8-10 September 2003*: 41-44.

Andriollo, M., Baccini, G., Martinelli, G., Morini, A. & Tortella, A. 2003b. Design optimisation of slotless linear PM motors. *LDIA 2003, Birmingham (UK), 8-10 September 2003*: 203-206.

Ansoft Co. 2005. *Maxwell® v.11, User guide.*